Gauss collocation methods for efficient structure preserving integration of post-Newtonian equations of motion

Jonathan Seyrich[*]

Mathematisches Institut, Universität Tübingen, Auf der Morgenstelle, 72076 Tübingen, Germany
(Received 23 February 2013; published 29 April 2013)

In this work, we present the hitherto most efficient and accurate method for the numerical integration of post-Newtonian equations of motion. We first transform the Poisson system as given by the post-Newtonian approximation to canonically symplectic form. Then we apply Gauss Runge-Kutta schemes to numerically integrate the resulting equations. This yields a convenient method for the structure preserving long-time integration of post-Newtonian equations of motion. In extensive numerical experiments, this approach turns out to be faster and more accurate (i) than previously proposed structure preserving splitting schemes and (ii) than standard explicit Runge-Kutta methods. We also show our approach to be appropriate for simulations on transitional precession.

I. INTRODUCTION

When Einstein gave birth to general relativity with the presentation of his field equations in 1915, new phenomena such as black holes and gravitational waves were soon predicted as consequences of this theory. In the last couple of years, gravitational waves have attracted ever more attention. With the aim to finally receive signals of such waves, much experimental effort has been put upon mounting land-based detectors. VIRGO in France and Italy (e.g., Ref. [1]), GEO 600 in Germany and the UK (e.g., Ref. [2]), KAGRA in Japan (e.g., Ref. [3]) and LIGO in the USA (e.g., Ref. [4]) are only to name a few. Perhaps they will one day be joined by the space-based eLISA [5]. In order to track any signal of gravitational waves, templates are required that give a hint on which needle to look for in the haystack of data delivered by all the working detectors. Such templates, in turn, can only be obtained by singling out the most promising sources of gravitational waves and calculating their motion in phase space. The main sources of waves have been identified to be binary systems consisting of inspiraling compact objects; see, e.g., Ref. [6]. Their mass proportions can be anything between equal masses and extreme ratios. Binaries with very unequal masses are called extreme mass ratio inspirals (EMRIs). One common example of an EMRI is a neutron star that orbits a super massive black hole. EMRIs allow for a simple description as a free particle (the lighter one) moving in a curved spacetime given by the metric corresponding to the mass of the heavier particle. Many possible shapes of the background metric have been proposed in this field (e.g., Refs. [7,8]).

Binaries with not so extreme a mass ratio are suitably described by the post-Newtonian (PN) formalism. This approach became possible after Arnowitt, Deser and Misner discovered that Einstein's theory can be formulated

as a Hamiltonian system [9]. The idea is then to expand the elements of the metric tensor and the equations of motion of the matter in powers of the small parameter $\frac{v^2}{c^2}$; see, e.g., Ref. [10]. This gives the Hamiltonian as a power series in the small parameter, the first term of the series being the Hamiltonian for Newton's law of gravitation. The determination of the individual terms in this expansion is subject to current research in theoretical physics, and contributions up to 3PN order have already been obtained some years ago via different approaches; see Refs. [11–18]. Very recently, contributions up to fourth order in the small parameter have been tackled; see Ref. [19]. Besides this, the post-Newtonian approach has been extended to a binary which is perturbed by a much lighter third body (e.g., Ref. [20]) and proper three-body PN Hamiltonians have been computed (e.g., Ref. [21]).

A property of relativistic test particles which is not known from classical mechanics is their spin. After the foundation for the treatment of this spin was laid down in the 1950s (e.g., Ref. [22]), the post-Newtonian formalism could be expanded to include the corresponding contributions. These comprise spin-orbit as well as spin-spin interactions; see, e.g., Refs. [23–27]. With this extension, the Hamiltonian system becomes a so-called Poisson system.

One important property of the post-Newtonian equations is that they are generally nonintegrable. As a consequence, the motion described by them can exhibit chaotic traits. If the motion of a particular binary is chaotic, the gravitational waves emitted during its inspiral will be unpredictable, thus leaving the researchers at the various wave detectors without any useful template. Hence, the investigation for chaos of a given binary system is an important task. Consequently, many works have been published concerning this topic both in the geodesic and the post-Newtonian field (e.g., Refs. [28–32]). The analysis of chaos requires reliable indicators and, above all, numerical simulations over very long time spans. Numerical long-term analysis, in turn, relies on there being efficient and

---

[*]seyrich@na.uni-tuebingen.de

highly accurate integration schemes which behave well even during long-time simulations. To this aim one can make use of the post-Newtonian equations' special structure.

Over the last few decades, the numerical analysis community came up with tools for the long-term integration of equations of motion. In the course of this, structure preserving algorithms such as symplectic schemes for Hamiltonian systems (e.g., Refs. [33–35]) or symmetric integrators for time-reversible systems (e.g., Refs. [36,37]) have been proposed. Regarding long-time behavior and conservation properties, these schemes are superior to ordinary numerical integrators such as explicit Runge-Kutta schemes in many applications of classical mechanics and astronomy. Whereas for standard integration schemes the overall error is normally proportional to the square of the length of the integration interval t_i, it only increases linearly with t_i for structure preserving integrators. And whereas there is a drift in constants of motions for standard methods, these constants are conserved up to a small error over extremely long times for symplectic algorithms. These algorithms have been successfully applied even in quantum mechanics. A comprehensive presentation of such methods is given by Hairer *et al.* [38].

In the last years, attempts have been made to construct structure preserving integrators for relativistic systems of compact binaries. Most recently, such a scheme has been proposed for the geodesic approximation; see Ref. [39]. In the realm of post-Newtonian equations, two different approaches have been considered so far. First, a noncanonically symplectic integrator has been constructed which preserves the system's Poisson structure; see Ref. [40]. Then, a transformation to canonical form has been proposed (see Ref. [41]), after which symplectic methods were applied [42]. All the previous approaches have in common that they are based on a splitting of the Hamiltonian into a Newtonian part and other relativistic contributions. In this work, we will first argue and then demonstrate via numerous experiments that a more efficient and accurate method for the solution of post-Newtonian equations consists of a transformation to symplectic form followed by the application of Gauss Runge-Kutta schemes. This will drastically reduce the numerical effort when simulating post-Newtonian systems. We will also be able to demonstrate that this approach yields the best results when applied to a test case showing transitional precession in the total angular momentum during the inspiral, a phenomenon which is of great interest to the gravitational wave community (e.g., Ref. [43]).

Our work is organized as follows: We first explain our notation in Sec. II. Afterwards we discuss the post-Newtonian equations of motion and their numerical properties in Sec. III. In Sec. IV we briefly summarize the main aspects of the Poisson integrator of Ref. [40]. Section V deals with the transformation to canonical form. Section VI presents common splitting methods. Then, in Sec. VII we present Gauss Runge-Kutta schemes and argue why they are a good choice in post-Newtonian simulations. Finally, we subject the individual methods to extensive tests, including a test case exhibiting transitional precession, and compare them to standard explicit schemes in Sec. VIII before we summarize our main results in Sec. IX.

II. NOTATION

In this work we use units such that $G = c = 1$. To facilitate the comparison with other works on the numerical treatment of post-Newtonian equations, we adapt our notation to the one introduced there (e.g., Refs. [40,42]). Thus, as the motion does not depend on the absolute value of the masses but on their ratio, we can, without loss of generality, assume the total mass $m := m_1 + m_2$ to be equal to 1 and introduce the reduced mass $\mu := \frac{m_1 m_2}{m}$, $q := \| \mathbf{x} \|$, $\nu := \frac{\mu}{m}$, and the unit vector $\mathbf{n} := \frac{\mathbf{x}}{q}$. Furthermore, we employ canonically conjugate position and momentum variables and restrict ourselves to the center-of-mass frame so that we have the relevant variables (with $a = 1$, 2 denoting the individual compact objects) $\mathbf{x} = \mathbf{x}_2 - \mathbf{x}_1$, $\mathbf{p} = \mathbf{p}_1 = -\mathbf{p}_2$, $\mathbf{S}_1$ and $\mathbf{S}_2$. For the sake of shorter notation we will combine the relevant variables of the phase space into one variable, $\mathbf{y} = (\mathbf{p}, \mathbf{x}, \mathbf{S}_1, \mathbf{S}_2)^T$. With this abbreviation we can write the equations of motion as

$$\frac{d\mathbf{y}}{dt} = f(\mathbf{y}), \qquad (1)$$

$$\mathbf{y}(0) = \mathbf{y}_0, \qquad (2)$$

with an appropriate function f. An exact solution of a differential equation of the form (1) which starts at a given point $\mathbf{y}_0$ and propagates the system over a time t will be denoted by

$$\mathbf{y}(t) = \varphi_t(\mathbf{y}_0), \qquad (3)$$

whereas a numerical approximated flow over a time step h is written as $\Phi_h(\mathbf{y}_0)$. Consequently, for a given point of the phase space $\mathbf{y}_n$, the next point on the numerical trajectory is calculated as

$$\mathbf{y}_{n+1} = \Phi_h(\mathbf{y}_n). \qquad (4)$$

Finally, I is a unit matrix of appropriate dimension and J is the symplecticity matrix

$$J = \begin{pmatrix} 0 & I \\ -I & 0 \end{pmatrix}. \qquad (5)$$

III. POST-NEWTONIAN EQUATIONS OF MOTION

We consider orbital contributions up to order 3PN as given in Ref. [15] and the leading term of the spin-orbit (SO) and the spin-spin (SS) contributions of Damour [26], respectively [44]. With all these terms, our Hamiltonian reads

$$H(\mathbf{p}, \mathbf{x}, \mathbf{S}_1, \mathbf{S}_2) = H_{orb}(\mathbf{p}, \mathbf{x}) + H_{SO}(\mathbf{p}, \mathbf{x}, \mathbf{S}_1, \mathbf{S}_2)$$
$$+ H_{SS}(\mathbf{p}, \mathbf{x}, \mathbf{S}_1, \mathbf{S}_2). \qquad (6)$$

The relevant terms of the orbital Hamiltonian H_{Orb} are

$$H_N(\mathbf{p}, \mathbf{x}) = \frac{\mathbf{p}^2}{2\mu} - \frac{\mu}{q}, \qquad (7)$$

$$H_{1PN,orb}(\mathbf{p}, \mathbf{x}) = \frac{1}{8\mu^3}(3\nu - 1)(\mathbf{p}^2)^2$$
$$- \frac{1}{2\mu^2 q}[(3 + \nu)\mathbf{p}^2 + \nu(\mathbf{n}\cdot\mathbf{p})^2] + \frac{\mu}{2q^2}, \qquad (8)$$

$$H_{2PN,orb}(\mathbf{p}, \mathbf{x}) = \frac{1}{16\mu^5}(1 - 5\nu 5\nu^2)(\mathbf{p}^2)^3$$
$$+ \frac{1}{8\mu^3 q}[(5 - 20\nu - 3\nu^2)(\mathbf{p}^2)^2 - 2$$
$$- \nu^2(\mathbf{n}\cdot\mathbf{p})^2\mathbf{p}^2 + 3\nu^2(\mathbf{n}\cdot\mathbf{p})^4]$$
$$+ \frac{1}{2\mu q^2}[3\nu(\mathbf{n}\cdot\mathbf{p})^2 + (5 + 8\nu)\mathbf{p}^2]$$
$$- \frac{(1 + 3\nu)\mu}{4q^3}, \qquad (9)$$

$$H_{3PN,orb}(\mathbf{p}, \mathbf{x}) = \frac{1}{128\mu^7}(-5 + 35\nu - 70\nu^2 + 35\nu^3)(\mathbf{p}^2)^4 + \frac{1}{16\mu^5 q}[(-7 + 42\nu - 53\nu^2 - 5\nu^3)(\mathbf{p}^2)^3$$
$$+ (2 - 3\nu)\nu^2(\mathbf{n}\cdot\mathbf{p})^2(\mathbf{p}^2)^2 + 3(1 - \nu)\nu^2(\mathbf{n}\cdot\mathbf{p})^4\mathbf{p}^2 - 5\nu^3(\mathbf{n}\cdot\mathbf{p})^6]$$
$$+ \frac{1}{16\mu^3 q^2}\left[(-27 + 136\nu + 109\nu^2)(\mathbf{p}^2)^2 + (17 + 30\nu)\nu(\mathbf{n}\cdot\mathbf{p})^2\mathbf{p}^2 + \frac{3}{4}(5 + 43\nu)\nu(\mathbf{n}\cdot\mathbf{p})^4\right]$$
$$+ \frac{1}{\mu q^3}\left\{\left[-\frac{25}{8} + \left(\frac{\pi^2}{64} - \frac{335}{48}\right)\nu - \frac{23}{8}\nu^2\right]\mathbf{p}^2 + \left(-\frac{85}{16} - \frac{3\pi^2}{64} - \frac{7\nu}{4}\right)\nu(\mathbf{n}\cdot\mathbf{p})^2\right\} + \frac{\mu}{q^4}\left[\frac{1}{8} + \left(\frac{109}{12} - \frac{21\pi^2}{32}\right)\nu\right]. \qquad (10)$$

The leading order spin-orbit coupling can be expressed by means of the orbital angular momentum $\mathbf{L} = \mathbf{x} \times \mathbf{p}$ and the effective spin

$$\mathbf{S}_{eff} = \left(1 + \frac{3m_2}{4m_1}\right)\mathbf{S}_1 + \left(1 + \frac{3m_1}{4m_2}\right)\mathbf{S}_2 \qquad (11)$$

as

$$H_{SO}(\mathbf{p}, \mathbf{x}, \mathbf{S}_1, \mathbf{S}_2) = 2\frac{\mathbf{S}_{eff} \cdot \mathbf{L}}{q^3}. \qquad (12)$$

The spin-spin interaction is the sum of the three following terms:

$$H_{S_1 S_2}(\mathbf{p}, \mathbf{x}, \mathbf{S}_1, \mathbf{S}_2) = \frac{1}{q^3}[3(\mathbf{S}_1 \cdot \mathbf{n})(\mathbf{S}_2 \cdot \mathbf{n}) - \mathbf{S}_1 \cdot \mathbf{S}_2], \qquad (13)$$

$$H_{S_1 S_1}(\mathbf{p}, \mathbf{x}, \mathbf{S}_1) = \frac{m_2}{2m_1 q^3}[3(\mathbf{S}_1 \cdot \mathbf{n})^2 - \mathbf{S}_1 \cdot \mathbf{S}_1], \qquad (14)$$

$$H_{S_2 S_2}(\mathbf{p}, \mathbf{x}, \mathbf{S}_2) = \frac{m_1}{2m_2 q^3}[3(\mathbf{S}_2 \cdot \mathbf{n})^2 - \mathbf{S}_2 \cdot \mathbf{S}_2]. \qquad (15)$$

Given the Hamiltonian, the dynamics of the system is described by the equations

$$\frac{d\mathbf{p}}{dt} = -\boldsymbol{\nabla}_{\mathbf{x}}H, \qquad (16)$$

$$\frac{d\mathbf{x}}{dt} = \boldsymbol{\nabla}_{\mathbf{p}}H, \qquad (17)$$

$$\frac{d\mathbf{S}_a}{dt} = (\boldsymbol{\nabla}_{\mathbf{S}_a}H) \times \mathbf{S}_a. \qquad (18)$$

These equations define a Poisson system for $\mathbf{y} = (\mathbf{p}, \mathbf{x}, \mathbf{S}_1, \mathbf{S}_2)^T$, i.e.,

$$\frac{d\mathbf{y}}{dt} = B(\mathbf{y})\boldsymbol{\nabla}H, \qquad (19)$$

with

$$B(\mathbf{y}) = \begin{pmatrix} 0 & -I & 0 & 0 \\ I & 0 & 0 & 0 \\ 0 & 0 & B_1(\mathbf{y}) & 0 \\ 0 & 0 & 0 & B_2(\mathbf{y}) \end{pmatrix}, \qquad (20)$$

$$B_1(\mathbf{y}) = \begin{pmatrix} 0 & -S_{1z} & S_{1y} \\ S_{1z} & 0 & -S_{1x} \\ -S_{1y} & S_{1x} & 0 \end{pmatrix}, \qquad (21)$$

$$B_2(\mathbf{y}) = \begin{pmatrix} 0 & -S_{2z} & S_{2y} \\ S_{2z} & 0 & -S_{2x} \\ -S_{2y} & S_{2x} & 0 \end{pmatrix}. \qquad (22)$$

A numerical scheme which preserves this special structure can be expected to have a benevolent long-time behavior similar to the symplectic case (e.g., Ref. [38]).

Furthermore, the post-Newtonian equations are in fact a perturbed Kepler problem, the corrections to the classical motion scaling with $\frac{1}{c^2}$. In the units $G = c = 1$ this scaling

is encoded in the higher orders of $\frac{1}{q}$ or $\mathbf{p}^2$ in the post-Newtonian terms. As $q > 1$ and $\mathbf{p}^2 < 1$ in most circumstances, one has a Hamiltonian of the form

$$H = H_{\mathrm{N}} + \delta\tilde{H}, \qquad \delta\tilde{H} \ll 1, \tag{23}$$

where the "larger" part can be solved analytically. Keeping in mind the just-mentioned properties of the post-Newtonian equations, we now present the already-known integration methods.

IV. POISSON INTEGRATOR FOR THE POST-NEWTONIAN EQUATIONS

The Poisson integrator suggested by Lubich *et al.* [40] is designed to exactly preserve the structure (19). Starting with the Hamiltonian (23), the relativistic contribution $\delta\tilde{H}$ is first split into an orbital part $H_{\mathrm{PN,orb}}$ and a spin term $H_{\mathrm{SO,SS}}$. The main idea is now to further decompose the spin-orbit and spin-spin parts as

$$H_{\mathrm{SO}} = H_{\mathrm{SO}}^x + H_{\mathrm{SO}}^y + H_{\mathrm{SO}}^z, \tag{24}$$

with

$$H_{\mathrm{SO}}^i = \frac{2}{q^3}(\mathbf{S}_{\mathrm{eff}} \cdot \hat{\mathbf{e}}_i)(\mathbf{L} \cdot \hat{\mathbf{e}}_i), \tag{25}$$

and

$$H_{\mathrm{SS}} = H_{\mathrm{SS}}^1 + H_{\mathrm{SS}}^2 + H_{\mathrm{SS}}^3 + H_{\mathrm{SS}}^4, \tag{26}$$

with

$$H_{\mathrm{SS}}^1 = -\frac{\mathbf{S}_1 \cdot \mathbf{S}_2}{q^3}, \tag{27}$$

$$H_{\mathrm{SS}}^2 = -\frac{\mathbf{S}_1 \cdot \mathbf{S}_1}{2q^3} - \frac{\mathbf{S}_2 \cdot \mathbf{S}_2}{2q^3}, \tag{28}$$

$$H_{\mathrm{SS}}^3 = \frac{3(\mathbf{S}_1 \cdot \mathbf{n})(\mathbf{S}_2 \cdot \mathbf{n})}{q^3}, \tag{29}$$

$$H_{\mathrm{SS}}^4 = \frac{3(\mathbf{S}_1 \cdot \mathbf{n})(\mathbf{S}_1 \cdot \mathbf{n})}{2q^3} + \frac{3(\mathbf{S}_2 \cdot \mathbf{n})(\mathbf{S}_2 \cdot \mathbf{n})}{2q^3}. \tag{30}$$

The major achievement of Lubich *et al.* [40] was to find analytical solutions φ_{SO}^i, φ_{SS}^i for the flow of each spin related part. This said, a structure preserving integrator $\Phi_{\mathrm{SO,SS}}$ for the spin terms is obtained by setting

$$\Phi_{\mathrm{SO,SS}} = \varphi_{\mathrm{SO}}^x \circ \varphi_{\mathrm{SO}}^y \circ \varphi_{\mathrm{SO}}^z \circ \varphi_{\mathrm{SS}}^1 \circ \varphi_{\mathrm{SS}}^2 \circ \varphi_{\mathrm{SS}}^3 \circ \varphi_{\mathrm{SS}}^4. \tag{31}$$

Thus, if one solves the flow φ_{N} of the Newtonian part analytically and uses a symplectic scheme to calculate the orbital relativistic contributions $\Phi_{\mathrm{PN,orb}}$, one can finally combine the three flows φ_{N}, $\Phi_{\mathrm{PN,orb}}$ and $\Phi_{\mathrm{SO,SS}}$ to obtain a structure preserving flow. In Sec. VI we will discuss how to best arrange the individual flows.

V. TRANSFORMATION TO CANONICAL FORM

Instead of directly preserving the Poisson structure (19) we can choose another way: The Darboux-Lie theorem states that for every Poisson system (19) one can find a transformation

$$\mathbf{z} = \Psi(\mathbf{y}), \tag{32}$$

such that the system in the coordinates $\mathbf{z}$ is locally canonical. There are two properties of the post-Newtonian equations which enable us to find such a transformation in this case. First, the positions and momenta are already in canonical form. Therefore, a transformation (32) only has to focus on the spin coordinates. Second, by multiplying the equations of motions of the spins (18) with the respective spin $\mathbf{S}_a$, we see that

$$\frac{1}{2}\frac{d\|\mathbf{S}_a\|}{dt} = \frac{d\mathbf{S}_a}{dt} \cdot \mathbf{S}_a = 0; \tag{33}$$

i.e., the length of the individual spins is a first integral. These two observations make it surprisingly easy to achieve the transformation to symplectic form.

From the constancy of the spin length we see that two spin variables are redundant. The post-Newtonian system can therefore be described by $N = 10$ variables. Because of this, Wu and Xie [41] proposed the use of cylindrical coordinates for the spins. Accordingly, we set

$$\mathbf{S}_a = m_a^2 \chi_a \begin{pmatrix} \rho_a \cos(\xi_a) \\ \rho_a \sin(\xi_a) \\ \xi_a \end{pmatrix}, \tag{34}$$

where χ_a relates the length of an object's spin to the square of its mass. The conservation of the spin length allows for the elimination of one of the variables (ρ_a, ϕ_a, ξ_a). Thus, we can express ρ_a in terms of ξ_a as

$$\rho_a = \sqrt{1 - \xi_a^2}, \tag{35}$$

whereby the spin and thus the Hamiltonian only depend on ϕ_a and ξ_a.

In order to deduce the equations of motion for the two independent variables, we observe that the following equalities hold true:

$$\frac{\partial H}{\partial \phi_a} = \frac{\partial H}{\partial S_{ax}}\frac{\partial S_{ax}}{\partial \phi_a} + \frac{\partial H}{\partial S_{ay}}\frac{\partial S_{ay}}{\partial \phi_a}, \tag{36}$$

$$\frac{\partial H}{\partial \xi_a} = \frac{\partial H}{\partial S_{ax}}\frac{\partial S_{ax}}{\partial \xi_a} + \frac{\partial H}{\partial S_{ay}}\frac{\partial S_{ay}}{\partial \xi_a} + \frac{\partial H}{\partial S_{az}}\frac{\partial S_{az}}{\partial \xi_a}, \tag{37}$$

$$\frac{\partial S_{ax}}{\partial \phi_a} = -\rho_a \sin(\phi_a) = -S_{ay}, \tag{38}$$

$$\frac{\partial S_{ay}}{\partial \phi_a} = \rho_a \cos(\phi_a) = S_{ax}, \tag{39}$$

$$S_{az} = \chi_a m_a^2 \xi_a. \tag{40}$$

For the sake of shorter notation, we assume without loss of generality that $\chi_a m_a^2 = 1$ until the end of this section.

Because of relation (40), we have

$$\frac{d\xi_a}{dt} = \frac{dS_{az}}{dt} = \frac{\partial H}{\partial S_{ax}} S_{ay} - \frac{\partial H}{\partial S_{ay}} S_{ax}, \tag{41}$$

where the second equality is simply the equation of motion for the z component of the spin. Substituting S_{ax} and S_{ay} with the help of Eqs. (38) and (39), and then applying (36) we get

$$\frac{d\xi_a}{dt} = -\frac{\partial H}{\partial S_{ax}} \frac{\partial S_{ax}}{\partial \phi_a} - \frac{\partial H}{\partial S_{ay}} \frac{\partial S_{ay}}{\partial \phi_a} = -\frac{\partial H}{\partial \phi_a}. \tag{42}$$

We now consider the time derivatives of the x and y components. Taking into account the equations of motion for these components, the derivatives with regard to time are

$$\frac{\partial H}{\partial S_{ay}} S_{az} - \frac{\partial H}{\partial S_{az}} S_{ay} = \frac{dS_{ax}}{dt} = \frac{\partial S_{ax}}{\partial \xi_a} \frac{d\xi_a}{dt} + \frac{\partial S_{ax}}{\partial \phi_a} \frac{d\phi_a}{dt}, \tag{43}$$

$$\frac{\partial H}{\partial S_{az}} S_{ax} - \frac{\partial H}{\partial S_{ax}} S_{az} = \frac{dS_{ay}}{dt} = \frac{\partial S_{ay}}{\partial \xi_a} \frac{d\xi_a}{dt} + \frac{\partial S_{ay}}{\partial \phi_a} \frac{d\phi_a}{dt}. \tag{44}$$

We can multiply the first equation by $\frac{\partial S_{ay}}{\partial \xi_a}$ and the second by $\frac{\partial S_{ax}}{\partial \xi_a}$ and subtract the two equations. This leads to

$$\left(\frac{\partial S_{ax}}{\partial \phi_a} \frac{\partial S_{ay}}{\partial \xi_a} - \frac{\partial S_{ay}}{\partial \phi_a} \frac{\partial S_{ax}}{\partial \xi_a}\right) \frac{d\phi_a}{dt}$$
$$= \frac{\partial H}{\partial S_{ay}} \frac{\partial S_{ay}}{\partial \xi_a} S_{az} - \frac{\partial H}{\partial S_{az}} \frac{\partial S_{ay}}{\partial \xi_a} S_{ay} - \frac{\partial H}{\partial S_{ay}} S_{az} \frac{\partial S_{ax}}{\partial \xi_a} S_{ax}$$
$$+ \frac{\partial H}{\partial S_{ax}} \frac{\partial S_{ax}}{\partial \xi_a} S_{az}. \tag{45}$$

Calculating the partial derivatives of the spin components with regard to the new variables on the left-hand side and some of the partial derivatives on the right-hand side, Eq. (45) becomes

$$\xi_a \frac{d\phi_a}{dt} = \frac{\partial H}{\partial S_{ay}} \frac{\partial S_{ay}}{\partial \xi_a} \xi_a + \frac{\partial H}{\partial S_{az}} \xi_a + \frac{\partial H}{\partial S_{ax}} \frac{\partial S_{ax}}{\partial \xi_a} \xi_a. \tag{46}$$

Keeping in mind that $\frac{\partial S_{az}}{\partial \xi_a} = 1$ and then making use of relation (37), we arrive at

$$\frac{d\phi_a}{dt} = \frac{\partial H}{\partial \xi_a}. \tag{47}$$

All in all, the post-Newtonian equations for the ten independent variables $\mathbf{z} = (\mathbf{p}, \xi_a, \mathbf{x}, \phi_a)$ read

$$\frac{d\mathbf{z}}{dt} = \frac{d}{dt} \begin{pmatrix} \mathbf{p} \\ \xi_1 \\ \xi_2 \\ \mathbf{x} \\ \phi_1 \\ \phi_2 \end{pmatrix} = \begin{pmatrix} 0 & -I \\ I & 0 \end{pmatrix} \begin{pmatrix} \boldsymbol{\nabla}_{\mathbf{p}} \\ \partial_{\xi_1} \\ \partial_{\xi_2} \\ \boldsymbol{\nabla}_{\mathbf{x}} \\ \partial_{\phi_1} \\ \partial_{\phi_2} \end{pmatrix} H, \tag{48}$$

which is to say that the system in the new variables is symplectic. What is more, the transformation is defined globally, as it is nothing other than expressing the spins with constant length via cylindrical coordinates. As a consequence, a structure preserving algorithm for the post-Newtonian equations can be obtained by carrying out the global transformation to canonical form and then applying a symplectic integrator.

VI. SCHEMES BASED ON SPLITTING

A. Splitting methods

It is well known (e.g., Ref. [45]) that, given a Hamiltonian of the form (23), an integrator which is split in this natural way has a smaller local error than a comparable scheme. More precisely, suppose we were given some second order method. We could apply it with a given step size h to the whole system (23), thus constructing the flow $\Phi_{H,h}$. But we could also apply the numerical scheme only to the "small" part $\delta \tilde{H}$ and combine this symmetrically with the flow φ_N of the first term in (23). This would yield the second order integrators

$$\Phi_{\text{split},h} = \varphi_{N,\frac{h}{2}} \circ \Phi_{\delta \tilde{H}, h} \circ \varphi_{N,\frac{h}{2}}, \tag{49}$$

and

$$\tilde{\Phi}_{\text{split},h} = \Phi_{\delta \tilde{H}, \frac{h}{2}} \circ \varphi_{N, h} \circ \Phi_{\delta \tilde{H}, \frac{h}{2}}. \tag{50}$$

Now, if we compared the local errors, we would get

$$\| \varphi_{H,h} - \Phi_{H,h} \| = \mathcal{O}(h^3) \tag{51}$$

for the numerical scheme applied to the whole system, but

$$\| \varphi_{H,h} - \Phi_{\text{split},h} \| = \mathcal{O}(\delta h^3), \tag{52}$$

$$\| \varphi_{H,h} - \tilde{\Phi}_{\text{split},h} \| = \mathcal{O}(\delta h^3), \tag{53}$$

for the splitting schemes. From this we observe that splitting can reduce a scheme's local error.

To see which of the two splitting methods is the better option, we first notice that, for post-Newtonian equations, the relativistic parts are nonseparable; i.e., the Hamiltonian cannot be split in the form

$$H(\mathbf{p}, \mathbf{x}) = T(\mathbf{p}) + V(\mathbf{x}). \tag{54}$$

Unfortunately, when a system is nonseparable, symplectic schemes have to be implicit; see, e.g., Ref. [38]. As a consequence, a splitting integrator of the form (50) has to

solve a system of implicit equations twice per time step, whereas a scheme of the form (49) leads to only one implicit system per step. Thus, the splitting $\Phi_{\text{split},h}$ can be expected to be more efficient than $\tilde{\Phi}_{\text{split},h}$. Numerical experiments by Zhong *et al.* [42] have confirmed this, so we will only consider splittings of the form (49) in the following.

B. Composition methods

The drawback of a splitting scheme is that—no matter if we choose (49) or (50)—it is of second order even if the numerical scheme for the $\delta\tilde{H}$ part is of (much) higher order. This can be overcome by clever composition: If we divide the step size h into smaller intervals $h = \alpha_1 h + \alpha_2 h + \alpha_3 h + \ldots$ and set for some second order method $\Phi_{\text{2nd},h}$

$$\Phi_{\text{comp},h} = \Phi_{\text{2nd},\alpha_1 h} \circ \Phi_{\text{2nd},\alpha_2 h} \circ \Phi_{\text{2nd},\alpha_3 h} \circ \ldots, \quad (55)$$

the thus-obtained scheme $\Phi_{\text{comp},h}$ will be of higher order, provided that the α_i satisfy specific conditions; see, e.g., Ref. [38], Chap. II. If the underlying second order scheme $\Phi_{\text{2nd},h}$ is symplectic, $\Phi_{\text{comp},h}$, as a composition of many symplectic operations, will be so, too.

Let us briefly state another useful fact about the implementation of composition schemes: If we choose the second order basic method as $\Phi_{\text{2nd},h} = \Phi_{\text{split},h}$, we have

$$\begin{aligned}
\Phi_{\text{comp},h} &= \ldots \circ \Phi_{\text{2nd},\alpha_i h} \circ \Phi_{\text{2nd},\alpha_{i+1} h} \circ \ldots \\
&= \ldots \circ \Phi_{\text{split},\alpha_i h} \circ \Phi_{\text{split},\alpha_{i+1} h} \circ \ldots \\
&= \ldots \circ \varphi_{N,\frac{\alpha_i h}{2}} \circ \Phi_{\delta\tilde{H},\alpha_i h} \circ \varphi_{N,\frac{\alpha_i h}{2}} \circ \varphi_{N,\frac{\alpha_{i+1} h}{2}} \\
&\quad \circ \Phi_{\delta\tilde{H},\alpha_{i+1} h} \circ \varphi_{N,\frac{\alpha_{i+1} h}{2}} \circ \ldots \\
&= \ldots \circ \varphi_{N,\frac{\alpha_i h}{2}} \circ \Phi_{\delta\tilde{H},\alpha_i h} \circ \varphi_{N,\frac{(\alpha_i + \alpha_{i+1})h}{2}} \circ \Phi_{\delta\tilde{H},\alpha_{i+1} h} \\
&\quad \circ \varphi_{N,\frac{\alpha_{i+1} h}{2}} \circ \ldots \quad (56)
\end{aligned}$$

In the last step we could "merge" terms thanks to the group property

$$\varphi_h \circ \varphi_s = \varphi_{h+s}, \quad (57)$$

which is valid for every exact flow, thus reducing the numerical effort. This would not be possible if we chose $\Phi_{\text{2nd},h} = \tilde{\Phi}_{\text{split},h}$ instead and, consequently, we found another advantage of splitting (49) over splitting (50).

One of the most popular composition methods is the state-of-the-art Suzuki composition [46],

$$\Phi_{\text{4th},h} = \Phi_{\text{2nd},\alpha h} \circ \Phi_{\text{2nd},\alpha h} \circ \Phi_{\text{2nd},\beta h} \circ \Phi_{\text{2nd},\alpha h} \circ \Phi_{\text{2nd},\alpha h}, \quad (58)$$

with

$$\alpha = \frac{1}{4 - 4^{\frac{1}{3}}}, \quad (59)$$

$$\beta = \frac{4^{\frac{1}{3}}}{4 - 4^{\frac{1}{3}}}. \quad (60)$$

This yields a fourth order method which is symmetric, i.e.,

$$\Phi_{\text{4th},h}^{-1} = \Phi_{\text{4th},-h}, \quad (61)$$

whenever the underlying scheme is. After all the background information on splitting and composition methods, we are now in the position to present structure preserving integration schemes for the post-Newtonian equations which have been considered so far.

C. Splitting schemes for post-Newtonian equations

We will present a Poisson integrator in accordance with Ref. [40] as well as a symplectic splitting scheme. In both cases we will use the implicit midpoint rule, already proposed in Ref. [34], which for any differential equation (1) has the form

$$\mathbf{y}_{n+1} = \mathbf{y}_n + h f\left(\frac{\mathbf{y}_n + \mathbf{y}_{n+1}}{2}\right). \quad (62)$$

It is of second order and preserves symmetry and symplecticity; see, e.g., Ref. [38].

(i) With the work of the previous two subsections and Sec. V, we construct a Poisson integrator as follows: We use the midpoint rule to calculate the flow $\Phi_{\text{PN,orb}}$ corresponding to the orbital relativistic contributions. Then, we use the flow corresponding to the spin related parts as given in (31) and its adjoint

$$\Phi_{\text{SO,SS}}^* = \Phi_{\text{SS}}^4 \circ \Phi_{\text{SS}}^3 \circ \Phi_{\text{SS}}^2 \circ \Phi_{\text{SS}}^1 \circ \Phi_{\text{SO}}^z \circ \Phi_{\text{SO}}^y \circ \Phi_{\text{SO}}^x, \quad (63)$$

and symmetrically combine them with $\Phi_{\text{PN,orb}}$ in the form

$$\Phi_{\delta\tilde{H},h}^{\text{Poisson}} = \Phi_{\text{SO,SS},\frac{h}{2}}^* \circ \Phi_{\text{PN,orb},h} \circ \Phi_{\text{SO,SS},\frac{h}{2}} \quad (64)$$

to obtain a numerical flow for all the relativistic parts $\delta\tilde{H}$ in (23). This numerical flow is symmetric and of second order as is any flow constructed in this way; see, e.g., Ref. [38], Chap. V. Therefore, we can combine it with the exact flow of the Newtonian part as in (49) to obtain the second order scheme

$$\Phi_{\text{split},h}^{\text{Poisson}} = \varphi_{N,\frac{h}{2}} \circ \Phi_{\delta\tilde{H},h}^{\text{Poisson}} \circ \varphi_{N,\frac{h}{2}}. \quad (65)$$

This said, we can apply Suzuki's composition (58) which yields the fourth order symmetric Poisson integrator

$$\begin{aligned}
\Phi_{\text{4th},h}^{\text{Poisson}} &= \Phi_{\delta\tilde{H},\alpha h}^{\text{Poisson}} \circ \Phi_{\delta\tilde{H},\alpha h}^{\text{Poisson}} \circ \Phi_{\delta\tilde{H},\beta h}^{\text{Poisson}} \circ \Phi_{\delta\tilde{H},\alpha h}^{\text{Poisson}} \\
&\quad \circ \Phi_{\delta\tilde{H},\alpha h}^{\text{Poisson}}. \quad (66)
\end{aligned}$$

(ii) In order to construct a symplectic scheme, we first apply the transformation to canonical form of

Sec. V. The Hamiltonian in the new variables $\mathbf{z}$ is still of the form (23). As a consequence, we can proceed along the lines of the two subsections above. Therefore, we apply the implicit midpoint rule to the whole relativistic contribution $\delta\tilde{H}$. This second order method can then be combined with the analytical solution of the Kepler problem, leading to the symplectic second order splitting scheme

$$\Phi_{\text{split},h}^{\text{sympl}} = \varphi_{N,\frac{h}{2}} \circ \Phi_{\delta\tilde{H},h}^{\text{midp}} \circ \varphi_{N,\frac{h}{2}}. \tag{67}$$

Again, we make use of Suzuki's composition and arrive at the integrator

$$\Phi_{4\text{th},h}^{\text{sympl}} = \Phi_{\delta\tilde{H},\alpha h}^{\text{sympl}} \circ \Phi_{\delta\tilde{H},\alpha h}^{\text{sympl}} \circ \Phi_{\delta\tilde{H},\beta h}^{\text{sympl}} \circ \Phi_{\delta\tilde{H},\alpha h}^{\text{sympl}}$$
$$\circ \Phi_{\delta\tilde{H},\alpha h}^{\text{sympl}}, \tag{68}$$

which is symplectic and of order 4.

The nice ideas behind them and their mathematical bounty notwithstanding, the just-presented structure preserving algorithms based on splitting methods are not very efficient: Even though we use the group property (57) to "merge" terms as illustrated in (56) whenever it is possible, the symplectic integrator $\Phi_{4\text{th},h}^{\text{sympl}}$ is still a composition of 11 flows, five of which can only be computed via the solution of ten-dimensional implicit systems. Using the Poisson integrator (66) instead, we also have to calculate the midpoint rule five times. As it is only applied to the orbital motion, the implicit systems are reduced to six dimensions. But for this we have to pay heavily because, taking everything together, we have to calculate 67 flows during one time step, most of which are related to the spin contributions and require the calculations of numerous rotations; see Ref. [40]. All these facts, which will be confirmed in the numerical experiments section below, make us look for a more efficient alternative to solve the post-Newtonian equations of motion. This is where Gauss collocation methods come into play.

VII. GAUSS RUNGE-KUTTA METHODS

Gauss Runge-Kutta methods are in fact collocation methods. Therefore, we give some background concerning these schemes.

A. Collocation polynomials

Given an interval $[t_0, t_0 + h]$, stages $0 \leq c_1 < \cdots < c_s \leq 1$, and an initial-value problem of the form (1), the polynomial $u(t)$ of degree s, satisfying

$$u(t_0) = \mathbf{y}_0, \tag{69}$$

$$\dot{u}(t_0 + c_i h) = f(t_0 + c_i h, u(t_0 + c_i h)), \quad i = 1, \ldots, s, \tag{70}$$

is called a collocation polynomial. In order to solve an initial-value problem by collocation, one has to find the polynomial $u(t)$ which satisfies the collocation conditions (69) and (70). This gives an approximate solution of the initial value problem after a time step h by setting

$$\mathbf{y}(t_0 + h)_{\text{col}} := u(t_0 + h). \tag{71}$$

A detailed introduction to collocation methods can be found in Ref. [47].

It can now readily be shown (e.g., Ref. [47]) that a collocation method is equivalent to an implicit s-stage Runge-Kutta scheme

$$\mathbf{y}_{n+1} = \mathbf{y}_n + h \sum_{i=1}^{s} b_i f(\mathbf{Y}_i), \tag{72}$$

$$\mathbf{Y}_i = \mathbf{y}_n + h \sum_{j=1}^{s} a_{ij} f(\mathbf{Y}_j), \tag{73}$$

with coefficients chosen as

$$a_{ij} = \int_0^{c_i} l_j(t) dt, \tag{74}$$

$$b_j = \int_0^1 l_i(t) dt. \tag{75}$$

Here, $l_i(t)$ denote the Lagrange polynomials of degree s,

$$l_i(t) = \prod_{i \neq j} \frac{t - c_j}{c_i - c_j}. \tag{76}$$

Depending on which set of stages $0 \leq c_1 < \cdots < c_s \leq 1$ is chosen, different collocation methods can be constructed. By setting

$$c_i = \frac{1}{2}(1 + \tilde{c}_i), \tag{77}$$

with $\tilde{c}_i$ being the roots of the Legendre polynomial of degree s, one obtains a Gauss collocation method. The order of this methods is $\mathcal{O}(h^{2s})$ (cf. Ref. [47]), which is optimal in the sense that there are no other s-stage one-step methods that achieve a similar high order without further numerical ruse. In addition, Gauss collocation methods are symplectic and time reversible, as is proven in Ref. [38]. Because of all these properties, Gauss Runge-Kutta methods are quite natural candidates for the solution of nonseparable Hamiltonian systems.

B. Gauss collocation for post-Newtonian equations

In order to employ Gauss Runge-Kutta methods in post-Newtonian simulations, we just have to conduct the transformation (32) of Sec. V and then apply a Gauss collocation scheme to the whole system in the new coordinates $\mathbf{z}$. Doing so, we will have to solve the system of implicit equations (73) for the inner stage values $\mathbf{Y}_i$ during each time step. This system has $s \cdot 10$ dimensions. Contrary to the splitting schemes, we have to solve the system only once when calculating the step $\mathbf{z}_n \rightarrow \mathbf{z}_{n+1}$.

Besides, we can drastically reduce the effort for the solution of the implicit system if we take account of the following.

C. Starting approximations

An implicit system has to be solved iteratively. Of course, the number of iterations necessary to obtain the solution depends on the distance between the starting guesses $\mathbf{Y}_i^0$ and the final values $\mathbf{Y}_i$. It would be beneficial, if there were a fast method to obtain guesses that are very close to the final values. This is possible for the Gauss collocations' implicit systems: Given the inner stage values of the last step $\mathbf{z}_{n-1} \to \mathbf{z}_n$, $\mathbf{Y}_i^{\text{laststep}}$, we set

$$\mathbf{Y}_i^0 = \mathbf{y}_{n-1} + h \sum_{j=1}^{s} \beta_{ij} f(\mathbf{Y}_j^{\text{last step}}). \qquad (78)$$

Note that this requires no additional function evaluation, as $f(\mathbf{Y}_j^{\text{last step}})$ had to be calculated in the previous step anyway. If the coefficients β_{ij} satisfy

$$\sum_{j=1}^{s} \beta_{ij} c_j^{k-1} = \frac{(1 + c_i)^k}{k}, \qquad k = 1, \ldots, s, \qquad (79)$$

one has (e.g., Ref. [38], Chap. VIII)

$$\| \mathbf{Y}_i - \mathbf{Y}_i^0 \| = \mathcal{O}(h^s), \qquad i = 1, \ldots, s. \qquad (80)$$

The above splitting schemes, in contrast, miss any similarly good starting approximations. Referring the interested reader to Ref. [48] where we have listed the coefficients c_i, b_i, a_{ij} and β_{ij} for $s = 2, 3, 4, 6$, we now move on to the numerical tests.

VIII. NUMERICAL EXPERIMENTS

All simulations for this work were run on a Core 2 Duo E6600 machine with 2.4 GHz and 4 GB RAM. The codes for the simulations have been written in $c++$.

In this section we test and compare the following algorithms:
  (i) Transformation to canonical form combined with Gauss Runge-Kutta methods for $s = 2, 3, 4$. The corresponding schemes are denoted by Gauss2, Gauss3, and Gauss4, respectively.
  (ii) The symplectic splitting scheme (68) which will be referred to as Symp.
  (iii) The Poisson integrator (66), abbreviated by Poiss.
  (iv) The classical fourth order explicit Runge-Kutta scheme given by the tableau

$$
\begin{array}{c|cccc}
0 & 0 & 0 & 0 & 0 \\
1/2 & 1/2 & 0 & 0 & 0 \\
1/2 & 0 & 1/2 & 0 & 0 \\
1 & 0 & 0 & 1 & 0 \\
\hline
 & 1/6 & 1/3 & 1/3 & 1/6.
\end{array}
\qquad (81)
$$

Hereafter, this method will by denoted by RK4.
  (v) The explicit Cash-Karp Runge-Kutta scheme

$$
\begin{array}{c|cccccc}
0 & & & & & & \\
1/5 & 1/5 & & & & & \\
3/10 & 3/40 & 9/40 & & & & \\
3/5 & 3/10 & -9/10 & 6/5 & & & \\
1 & -11/54 & 5/2 & -70/27 & 35/27 & & \\
7/8 & 1631/55296 & 175/512 & 575/13824 & 44275/110592 & 253/4096 & \\
\hline
 & 37/378 & 0 & 250/621 & 125/594 & 0 & 512/1771,
\end{array}
\qquad (82)
$$

as proposed by Press *et al.* [49], which is of order 5 and will be abbreviated by CK5.

As the most reasonable measure for the efficiency, we compare the CPU calculation times. The algorithms' accuracy is tested with the help of the relative error in the Hamiltonian,

$$\Delta H = \left| \frac{H(\mathbf{y}_n) - H(\mathbf{y}_0)}{H(\mathbf{y}_0)} \right|, \qquad (83)$$

and the relative error along the trajectory,

$$\text{err} = \sqrt{\sum_{i=1}^{N} \left(\frac{y_{\text{num}}^i - y_{\text{ex}}^i}{y_{\text{ex}}^i} \right)^2}. \qquad (84)$$

Here, the superscript i denotes a vector's ith component. Unless stated otherwise, the "exact" solution $\mathbf{y}_{\text{ex}}(t)$ will be given by an $s = 6$-stage Gauss Runge-Kutta scheme with a step size $h = 0.1$ applied to the system in canonical coordinates.

The simulations are aborted due to poor accuracy as soon as the error in the energy exceeds the tolerance

$$\Delta H > 10^{-6}. \qquad (85)$$

At first glance, it seems arbitrary to subject the integrators to such an upper limit on the energy error. But we will show now that such a bound is indeed necessary.

A. The importance of energy conservation

Let us assume there was no upper limit on the error in the energy and we applied RK4 to the orbital test case. For different step sizes h, this would yield the energy errors as given in Fig. 1. Let us now further assume we wanted to plot Poincaré sections for this two-dimensional problem in order to investigate it for chaotic behavior. For different h, we would obtain the sections plotted in Fig. 2. For large h, these resemble chaotic rather than the correct quasiperiodic motion.

Applying Gauss3 with the large step size $h = 40$ instead, the energy is conserved, and consequently, the sections are calculated correctly (cf. Fig. 3). We have thus
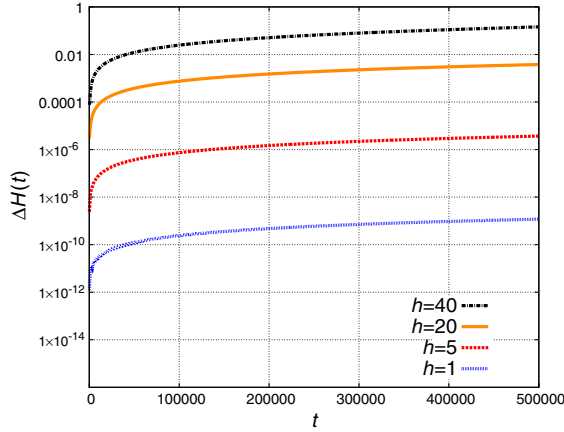
FIG. 1 (color online). For the classical RK4 scheme applied with different step sizes h to the purely orbital test case, the error in the energy ΔH is plotted against integration time t.
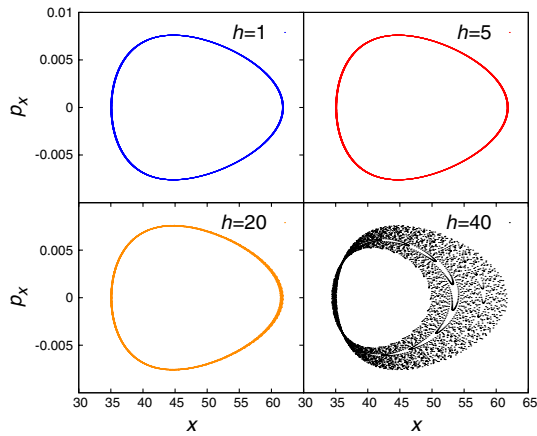

FIG. 2 (color online). Poincaré sections at $y = 0$, $p_y > 0$ for the purely orbital test case obtained with RK4 and four different step sizes h.
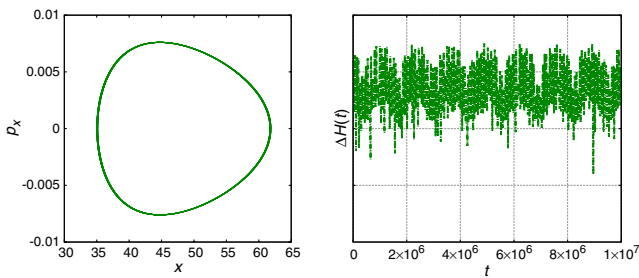

FIG. 3 (color online). The left panel shows Poincaré sections at $y = 0$, $p_y > 0$ for the purely orbital test case obtained with Gauss3 and $h = 40$. In the right panel, the corresponding error in the energy ΔH is plotted against integration time t.

illustrated that a threshold for the relative error in the energy is inevitable if we want to obtain reliable information on the chaoticity. Let us now present the test cases with the help of which we compare the individual methods.

B. The test cases

We model three different kinds of motion, each of which is often encountered in binary simulations. We always fix the total mass as $m = 1$. Consequently, the important parameter concerning the two compact objects' masses is the mass ratio $\sigma = \frac{m_1}{m_2}$. The individual masses and the reduced mass are thus given as

$$m_1 = \frac{\sigma}{1 + \sigma}, \tag{86}$$

$$m_2 = \frac{1}{1 + \sigma}, \tag{87}$$

$$\mu = \frac{\sigma}{(1 + \sigma)^2}. \tag{88}$$

The other relevant parameter is the factor χ_a, already introduced in Sec. V, that links masses with spins via

$$\|\mathbf{S}_a\| = \chi_a m_a^2. \tag{89}$$

Hence, the nature of a binary's orbit depends on the parameters σ, χ_1, χ_2 and the initial values

$$\mathbf{z}(0) = (p_x(0), p_y(0), p_z(0), \xi_1(0), \xi_2(0), x(0), y(0),$$
$$z(0), \phi_1(0), \phi_2(0))^T. \tag{90}$$

This said, the three kinds of motion are represented by the following respective examples:

(i) With the set of initial data

$$\mathbf{z}(0) = \left(0, \frac{3}{80}, 0, 0, 0, 35, 0, 0, 0, 0\right)^T, \qquad \sigma = \frac{1}{3},$$
$$\chi_1 = \chi_2 = 0, \tag{91}$$

we model a system without spin effects. The spin contributions being switched off, the post-Newtonian system is integrable (e.g., Ref. [41]), and the motion is restricted to the initial plane due to the conservation of the angular momentum. We present the orbit and the Poincaré sections for $t \in [0, 10^7]$ as obtained via "exact" integration in Fig. 4. The motion is apparently quasiperiodic.

(ii) As a second test case, we choose the data set

$$\mathbf{z}(0) = \left(0, \frac{3}{80}, 0, 0.25, -0.025, 35, 0, 0, \frac{\pi}{4}, \frac{\pi}{4}\right)^T,$$
$$\sigma = \frac{1}{3}, \qquad \chi_1 = \chi_2 = \frac{3}{4}. \tag{92}$$

In Fig. 5, we plot a part of the orbital trajectory for $t \in [0, 10^7]$. Alongside this, we plot the frequency spectrum of the x component for $I_1 = [0, 10^6]$ and $I_2 = [10^7 - 10^6, 10^7]$. We see that, although the spin contributions have been switched on, the motion is still regular.

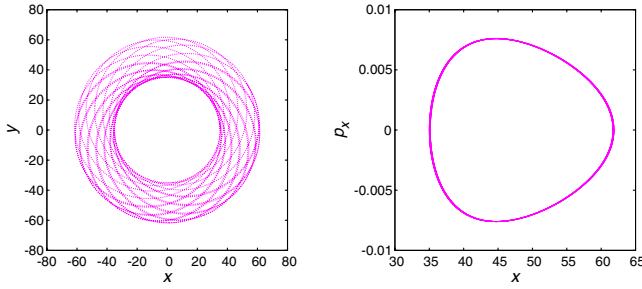(iii) We also consider a chaotic orbit. More precisely, we set

FIG. 4 (color online). For the test case without spin contributions and $t \in [0, 10^7]$, the left panel shows an extract of the trajectory. The Poincaré sections for $y = 0$ and $p_y > 0$ are given in the right panel.
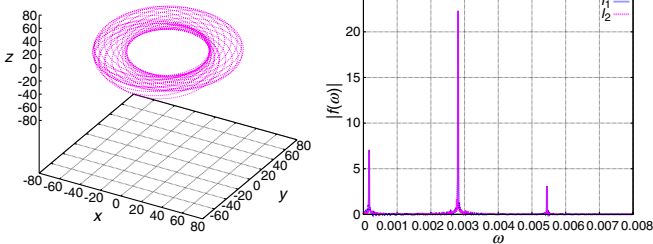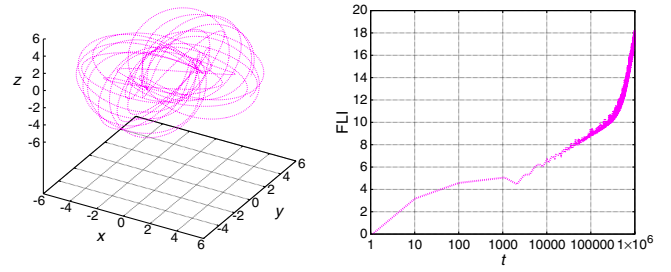

FIG. 6 (color online). For the chaotic test case, the left panel shows the trajectory for $t \in [0, 25000]$. The linearly growing FLI is depicted in the right panel in semilogarithmic scale.

FIG. 5 (color online). For the test case (92), the left panel shows the trajectory for $t \in [0, 50000]$. The frequency spectra $|f^x(\omega)|$ for the time intervals $I_1 = [0, 10^6]$ and $I_2 = [10^7 - 10^6, 10^7]$ are depicted in the right panel.

$$\mathbf{z}(0) = \left(0, \frac{3}{40}, 0, 0.25, -0.025, 6, 0, 0, \frac{\pi}{4}, \frac{\pi}{4}\right)^T,$$
$$\sigma = 1, \qquad \chi_1 = \chi_2 = 1. \qquad (93)$$

We illustrate the chaotic behavior by showing a part of the orbital trajectory and the fast lyapunov indicator (FLI) in Fig. 6. The FLI shows characteristically chaotic traits (cf. Ref. [50]).

Having thus established the test cases, we are able to start with our experiments.

C. Comparing the splitting schemes

We first compare the two splitting schemes. As they are exactly the same in the nonspinning case, we turn towards the regular spinning example (92) and plot the respective error in the Hamiltonian for various h in Fig. 7. We see no difference in the accuracy. But when comparing the corresponding calculation times in Table I, we see that the Poisson scheme is much slower.

Testing the splitting schemes for the chaotic test case, we see that Symp falls victim to criterion 85 for step sizes as small as $h = 5$, but it can cope with it for $h < 1$. This is not so for Poiss which even fails for $h = 0.01$. Consequently, the symplectic splitting (68) is superior to the Poisson integrator (66). But as we will
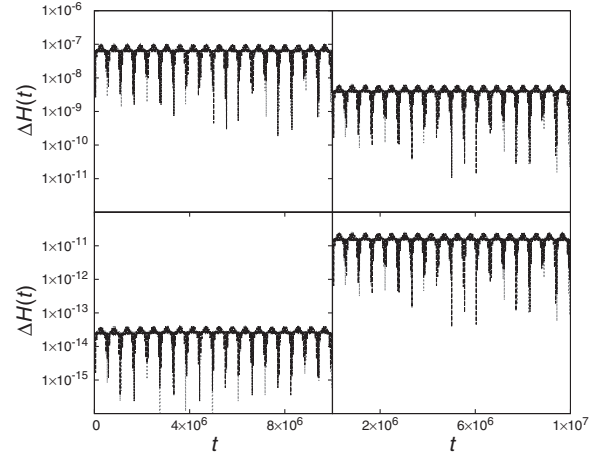

FIG. 7. For initial data (92), $t \in [0, 10^7]$ and different step sizes h, the relative error in the Hamiltonian ΔH is plotted against time t for the splitting integrators of Sec. VIC. No difference can be spotted between them.

corroborate now, it is by no means the best option for post-Newtonian systems.

D. Comparing integration schemes

Here, we compare the symplectic splitting to the (explicit and structure preserving) Runge-Kutta schemes. First, we list the calculation times for simulations with the orbital test case in Table II. As would have been expected, the explicit schemes are faster than the other methods for equal step sizes. But they have to be applied with small step sizes in order not to hurt the constraint on the energy error. We also see that Symp is by far the slowest algorithm.

TABLE I. The CPU calculation times in [s] for the two splitting integrators applied to the regular, spinning test case (92) with different step sizes h. The integration interval was $t \in [0, 10^7]$ in all simulations.

Integrator	$h = 40$	$h = 20$	$h = 5$	$h = 1$
Symp	9.90	18.72	67.75	304.95
Poiss	17.37	34.23	133.34	655.11

TABLE II. The CPU calculation times in [s] for several schemes applied to the orbital test case (92) with different step sizes h. The integration interval was $t \in [0, 10^7]$ in all simulations. "a" signifies "aborted due to condition (85)."

Integrator	$h = 40$	$h = 20$	$h = 5$	$h = 1$	$h = 0.5$	$h = 0.1$
RK4	a	a	a	13.80	27.58	137.91
CK5	a	a	4.70	23.01	46.07	230.01
Gauss2	a	3.89	11.44	43.81	81.73	344.41
Gauss3	3.27	5.32	15.44	58.48	105.73	422.69
Gauss4	3.96	6.47	18.74	67.26	120.59	443.49
Symp	4.36	8.35	30.95	142.86		

Doing the same observations for the regular spinning case, we get equal results, cf. Table III.

As the errors of the individual integrators behave similarly for both regular orbits, we only show the case with spins included. We plot the error along the trajectory 84 in Fig. 8 and the relative error in the Hamiltonian 83 in Fig. 9. We see that, although Symp is more accurate than CK5 and Gauss2 with equal step sizes, it has a larger error than the much faster Gauss3 and Gauss4 with equal or even much larger step sizes.

We now turn our attention towards the chaotic motion arising from the initial conditions (93). Again, we start with listing the calculation times of simulations with various step sizes in Table IV, right after which we plot the error along the trajectory in Fig. 10 and the relative error in the energy for various simulations in Fig. 11. The first point to mention here is that the explicit methods require prohibitively small step sizes in order not to exceed the error bar (85). As of the structure preserving candidates, the result is qualitatively the same as in the regular simulations: Symp seems to be better than Gauss2, which struggles with the chaotic case. But it obviously cannot match the performance of the fast and accurate Gauss3 and Gauss4.

One interesting point which stands out for all three initial data is that the difference in CPU times between explicit and Gauss Runge-Kutta schemes decreases for smaller step sizes. This is thanks to the starting approximations introduced in Sec. VII C. The smaller the step size, the closer the initial guess of the iterations gets to the correct values due to relation (80). Consequently, the average number of
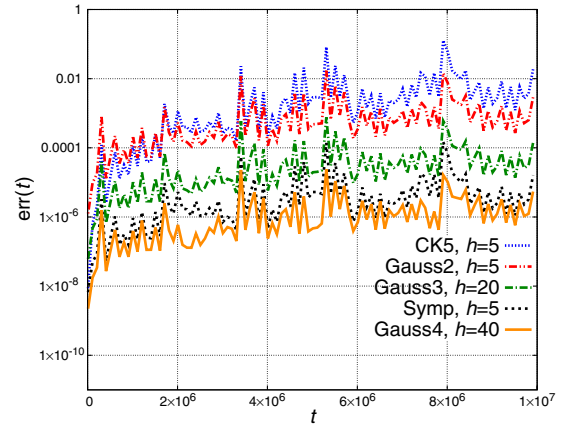

FIG. 8 (color online). For initial data (92) and $t \in [0, 10^7]$, the relative error along the trajectory [cf. (84)] is plotted against time t for various integration schemes.
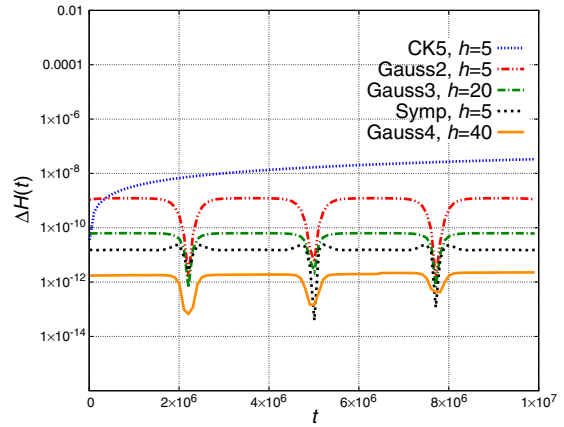

FIG. 9 (color online). For initial data (92) and $t \in [0, 10^7]$, the relative error in the Hamiltonian ΔH is plotted against time t for various integration schemes.

iterations per step decreases alongside h. To illustrate this, we list the iterations per step of Gauss4 in Table V.

We have seen that the structure preserving algorithms have excellent conservation properties when applied to symplectic systems. What will happen if we add a radiation term to the binary system?

TABLE III. The CPU calculation times in [s] for several schemes applied to the regular, spinning test case (92) with different step sizes h. The integration interval was $t \in [0, 10^7]$ in all simulations. "a" signifies "aborted due to condition (85)."

Integrator	$h = 40$	$h = 20$	$h = 5$	$h = 1$	$h = 0.5$	$h = 0.1$
RK4	a	a	a	43.99	87.93	439.44
CK5	a	a	14.31	71.56	143.02	716.16
Gauss2	a	10.03	29.37	111.23	205.68	852.88
Gauss3	8.10	13.19	38.09	141.19	255.60	997.65
Gauss4	10.00	16.44	46.63	160.95	283.26	1068.56
Symp	9.90	18.72	67.75	304.95		

TABLE IV. The CPU calculation times in [s] for several schemes applied to the chaotic test case (92) with different step sizes h. The integration interval was $t \in [0, 10^7]$ in all simulations. "a" signifies "aborted due to condition (85)."

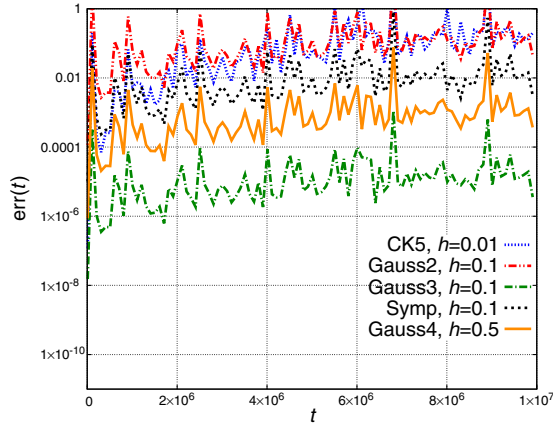| Integrator	$h = 5$	$h = 1$	$h = 0.5$	$h = 0.1$	$h = 0.05$	$h = 0.01$
RK4	a	a	a	a	a	2997.76
CK5	a	a	a	a	a	4840.96
Gauss2	a	a	a	1190.14		
Gauss3	a	a	449.47	1548.56		
Gauss4	a	347.22	566.67	1893.45		
Symp	a	463.78	833.85	3445.49		

FIG. 10 (color online). For initial data (93), the relative error along the trajectory [cf. (84)] is plotted against time t for various integration schemes.
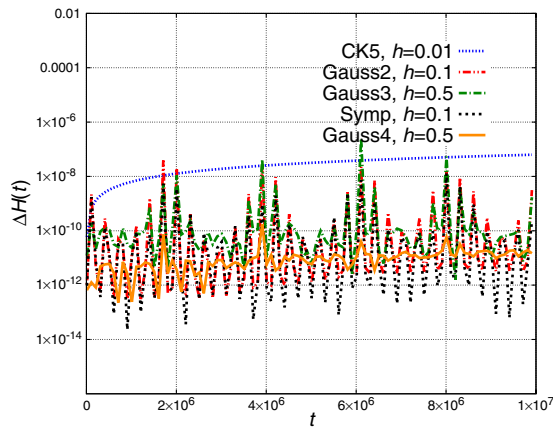

FIG. 11 (color online). For initial data (93) and $t \in [0, 10^7]$, the relative error in the Hamiltonian ΔH is plotted against time t for various integration schemes.

E. Systems with radiation

Adding a dissipative term, the system loses the structure which gave rise to the advantageous integrators in the first place. But it is known from classical mechanics that, at least in this field, structure preserving algorithms outperform explicit schemes also when a nonconservative term is added to the Hamiltonian. In order to examine the corresponding behavior for relativistic binaries, we restrict ourselves to the initial data (92) and modify the equation of
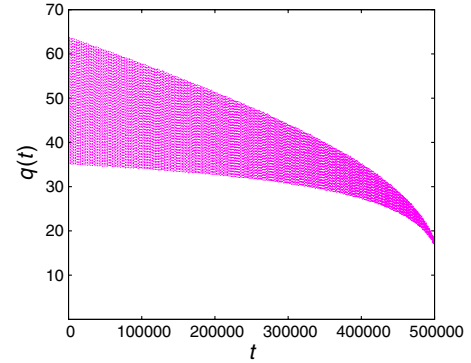

FIG. 12 (color online). The radial distance q as a function of integration time t for the regular spinning orbit with radiation effects included.

motion of the momenta (16) to account for radiation. We choose a model for the radiation force F_{rad} derived by Buonanno *et al.* [51] which is commonly used in general relativity and set

$$\frac{d\mathbf{p}}{dt} = -\nabla_{\mathbf{x}}H + \mathbf{F}_{rad}. \qquad (94)$$

To illustrate its effects on the trajectory, we plot the evolution of the radial distance q for our regular, spinning test case (92) as given by the exact solution in Fig. 12. Here, we calculate the "exact" solution with CK5 and the very small step size $h = 0.01$. As time increases, the distance between the two particles is decreasing faster and faster. For $t > 500\,000$, the post-Newtonian approximation will soon lose its validity. Thus, we restrict our simulations to an interval $t \in [0, 500\,000]$.

In the subsections above, CK5 and Gauss3/Gauss4 showed the best results for explicit and structure preserving schemes, respectively. We thus focus on these integrators and compare their performance with the radiation turned on. We first list the calculation times for the three schemes applied with different step sizes each, cf. Table VI. With increasing time steps, the difference in CPU time becomes ever smaller as the collocation methods' average number of iterations per step decreases analogously to the conservative case.

As a measure for the accuracy we plot the relative error along the trajectory 84 in Fig. 13. Taking into account the calculation times, the collocation methods yield the better

TABLE V. Number of iterations per step for Gauss4, applied with different step sizes to the three test cases. "a" signifies "aborted due to condition (85)."

Test case	$h = 40$	$h = 20$	$h = 5$	$h = 1$	$h = 0.5$	$h = 0.1$
Initial values (91)	9.19	7.44	5.16	3.46	2.99	2.13
Initial values (92)	9.31	7.59	5.30	3.54	3.07	2.24
Initial values (93)			a	9.21	7.44	4.85

TABLE VI. The CPU calculation times in [s] for explicit and implicit Runge-Kutta schemes applied with different step sizes h to the test case (92) with radiation effects included. The integration interval was $t \in [0, 500\,000]$ for all simulations.

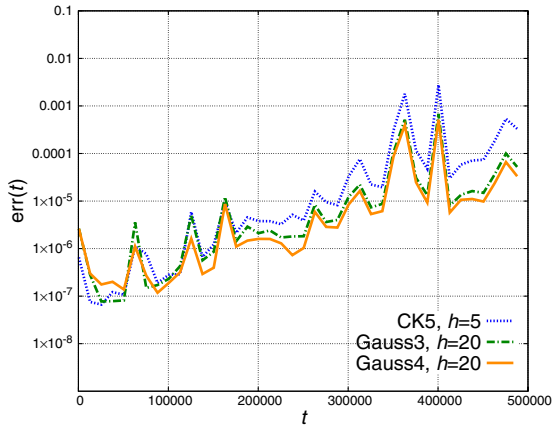| Integrator	$h = 40$	$h = 20$	$h = 5$	$h = 1$	$h = 0.5$	$h = 0.1$
CK5	0.14	0.28	1.21	5.75	11.50	57.51
Gauss3	0.92	1.47	4.04	16.45	25.69	99.77
Gauss4	1.08	1.72	4.72	17.28	32.00	133.36

FIG. 13 (color online). The relative error along the trajectory, err, against integration time t for explicit and collocation schemes applied to the system with radiation included.

results for less computational costs—just as in the conservative case.

F. Systems which exhibit transitional precession

As a last point, we show that the new integration method is appropriate for investigations on transitional precession of binary systems. This form of precession is exhibited by binaries whose orbital and spin angular momenta are anti-aligned and of approximately equal magnitude; see Ref. [43] for detailed information on the topic. As appropriate initial conditions, we choose (cf. Ref. [43], Fig. 17)

$$\mathbf{z}(0) = \left(0, \frac{1}{\sqrt{75}}, 0, -0.99939, 0, 75, 0, 0, \frac{\pi}{4}, \frac{\pi}{4}\right)^T,$$

$$\sigma = \frac{1}{0.13}, \qquad \chi_1 = 1, \qquad \chi_2 = 0, \tag{95}$$

which we subject to the same equations of motion as in Sec. VIII E. We compare the same three integration schemes as in the previous subsection. Their respective accuracy is now measured by means of the relative error of the total angular momentum

$$\mathbf{J} = \mathbf{L} + \mathbf{S}_1 + \mathbf{S}_2, \tag{96}$$

which is the quantity of interest in works such as Ref. [43]. Thus, in Fig. 14 we plot the relative error

$$\mathrm{err}_J = \sqrt{\sum_{i=1}^{3} \left(\frac{J_{\mathrm{ex}}^i - J_{\mathrm{num}}^i}{J_{\mathrm{ex}}^i}\right)^2} \tag{97}$$

against the integration time t for the three methods. The "exact" solution is again obtained by a simulation with CK5 and $h = 0.01$. Again, the implicit Gauss Runge-Kutta schemes show a smaller error even for much larger time steps. A comparison of the integration times yields the same results as in the previous subsection and, hence,
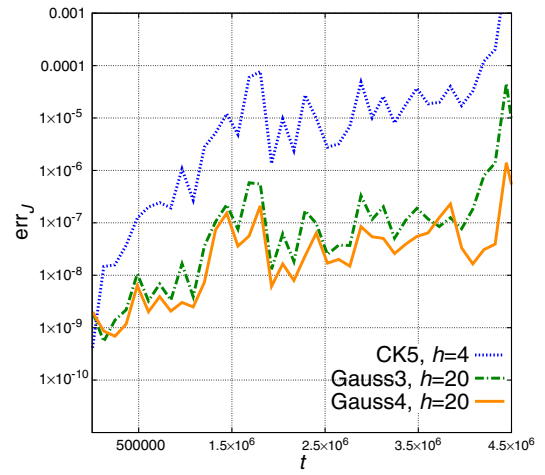

FIG. 14 (color online). The relative error of the total angular momentum, err$_J$, against integration time t for explicit and collocation schemes applied to a system which exhibits transitional precession.

Gauss Runge-Kutta schemes are the best choice for simulations concerning transitional precession.

IX. SUMMARY

We have seen that structure preserving algorithms are necessary for the long-time integration of post-Newtonian equations of motion, as they guarantee the conservation of the energy which is inevitable in investigations for chaos. Thus, in this work we analyzed several algorithms—a Poisson integrator based on the Poisson structure, a symplectic splitting scheme and Gauss Runge-Kutta methods. We observed large discrepancies in the performance of the individual structure preserving methods. Some even fared worse than explicit methods. More specifically, the Poisson integrator turned out to be extremely slow when applied to our test cases. The symplectic scheme based on state-of-the-art splitting and composition techniques could compete with a Gauss Runge-Kutta scheme with two inner stages but was completely inferior to Gauss collocation schemes with three or more inner stages. These Gauss methods turned out to be by far the most efficient and most accurate option. Even for dissipative systems, including systems exhibiting transitional precession in the total angular momentum, they delivered more accurate results for equal computational cost than high order explicit Runge-Kutta schemes. Therefore, we strongly recommend using a transformation of the system to symplectic form combined with a Gauss Runge-Kutta scheme for the numerical long-time analysis of post-Newtonian systems.

ACKNOWLEDGMENTS

[1] A. Giazotto, Nuovo Cimento C **15**, 955 (1992); http://www.virgo.infn.it.

[2] H. Lück and GEO600 Team, Classical Quantum Gravity **14**, 1471 (1997); http://www.geo600.uni-hannover.de.

[3] K. Kuroda and LCGT Collaboration, Classical Quantum Gravity **27**, 084004 (2010); http://gwcenter.icrr.u-tokyo.ac.jp/en/.

[4] A. Abromovici, W. E. Althouse, R. W. P. Drever, Y. Gürsel, S. Kawamura, F. J. Raab, D. Shoemaker, L. Sievers, R. E. Spero, K. S. Thorne, R. E. Vogt, R. Weiss, S. E. Whitcomb, and M. E. Zucker, Science **256**, 325 (1992); http://www.ligo.caltech.edu.

[5] http://www.elisa-ngo.org.

[6] L. Blanchet, Living Rev. Relativity **5**, 3 (2002).

[7] V. S. Manko, J. D. Sanabria-Gómez, and O. V. Manko, Phys. Rev. D **62**, 044048 (2000).

[8] R. P. Kerr and A. Schild, Gen. Relativ. Gravit. **41**, 2485 (2009).

[9] R. Arnowitt, S. Deser, and C. W. Misner, Gen. Relativ. Gravit. **40**, 1997 (2008).

[10] G. Schäfer, Banach Center publications **41**, 43 (1997).

[11] P. Jaranowiski and G. Schäfer, Phys. Rev. D **57**, 7274 (1998).

[12] T. Damour, P. Jaranowiski, and G. Schäfer, Phys. Rev. D **62**, 044024 (2000).

[13] P. Jaranowiski and G. Schäfer, Phys. Rev. D **63**, 029902 (2000).

[14] T. Damour, P. Jaranowiski, and G. Schäfer, Phys. Rev. D **63**, 029903 (2000).

[15] T. Damour, P. Jaranowiski, and G. Schäfer, Phys. Lett. B **513**, 147 (2001).

[16] L. Blanchet and G. Faye, J. Math. Phys. (N.Y.) **41**, 7675 (2000).

[17] L. Blanchet and G. Faye, Phys. Lett. A **271**, 58 (2000).

[18] L. Blanchet and G. Faye, Phys. Rev. D **63**, 062005 (2001).

[19] P. Jaranowiski and G. Schäfer, Phys. Rev. D **86**, 061503 (2012).

[20] P. Galaviz and B. Brügmann, Phys. Rev. D **83**, 084013 (2011).

[21] G. Schäfer, Phys. Lett. **123A**, 336 (1987).

[22] A. Papapetrou, Proc. R. Soc. A **209**, 248 (1951).

[23] B. M. Barker and R. F. O'Connell, Phys. Rev. D **2**, 1428 (1970).

[24] B. M. Barker and R. F. O'Connell, Phys. Rev. D **12**, 329 (1975).

[25] T. Damour and G. Schäfer, Nuovo Cimento B **101**, 127 (1988).

[26] T. Damour, Phys. Rev. D **64**, 124013 (2001).

[27] T. Damour, P. Jaranowiski, and G. Schäfer, Phys. Rev. D **77**, 064032 (2008).

[28] G. Lukes-Gerakopoulos, T. A. Apostolatos, and G. Contopoulos, Phys. Rev. D **81**, 124005 (2010).

[29] W.-B. Han, Phys. Rev. D **77**, 123007 (2008).

[30] A. Gopakumar and C. Königsdörffer, Phys. Rev. D **71**, 024039 (2005).

[31] N. J. Cornish and J. Levin, Phys. Rev. D **68**, 024004 (2003).

[32] X. Wu and Y. Xie, Phys. Rev. D **76**, 124004 (2007).

[33] R. D. Ruth, IEEE Trans. Nucl. Sci. **30**, 2669 (1983).

[34] K. Feng, Journal of Computational Mathematics **4**, 279 (1986).

[35] E. Hairer, C. Lubich, and G. Wanner, Acta Numer. **12**, 399 (2003).

[36] P. C. Hammer and J. W. Hollingsworth, Mathematical Tables and Other Aids to Computation **9**, 92 (1955).

[37] E. Hairer and G. Söderlind, SIAM J. Sci. Comput. **26**, 1838 (2005).

[38] E. Hairer, C. Lubich, and G. Wanner, *Geometric Numerical Integration. Structure-Preserving Algorithms for Ordinary Differential Equations* (Springer, Berlin, 2006), 2nd ed.

[39] J. Seyrich and G. Lukes-Gerakopoulos, Phys. Rev. D **86**, 124013 (2012).

[40] C. Lubich, B. Walther, and B. Brugmann, Phys. Rev. D **81**, 104025 (2010).

[41] X. Wu and Y. Xie, Phys. Rev. D **81**, 084045 (2010).

[42] S. Y. Zhong, X. Wu, S.-Q. Liu, and X.-F. Deng, Phys. Rev. D **82**, 124040 (2010).

[43] T. A. Apostolatos, C. Cutler, G. J. Sussman, and K. S. Thorne, Phys. Rev. D **49**, 6274 (1994).

[44] Although in the presentation of this work we restrict ourselves to first order terms of SO and SS coupling, we remark that the symplectic schemes also work for higher order spin terms such as those in Ref. [26]. Comparing various symplectic integration schemes would yield the same results as the ones presented here.

[45] X. Liao, Celest. Mech. Dyn. Astron. **66**, 243 (1997).

[46] M. Suzuki, Phys. Lett. **165A**, 387 (1990).

[47] E. Hairer, S. P. Nørsett, and G. Wanner, *Solving Ordinary Differential Equations I* (Springer, Berlin, 1993), 2nd ed.

[48] A file gauss_coefficients.txt can be found on http://na.uni-tuebingen.de/~seyrich/.

[49] W. Press, S. Teukolsky, W. Vetterling, and B. Flannery, *Numerical Recipes in C. The Art of Scientific Computing* (Cambridge University Press, Cambridge, England, 1992), 2nd ed.

[50] X. Wu, T. Y. Huang, and H. Zhang, Phys. Rev. D **74**, 083001 (2006).

[51] A. Buonanno, Y. Chen, and T. Damour, Phys. Rev. D **74**, 104005 (2006).